Reassessment of the sulfur and halogen emissions from the Millennium Eruption of Changbaishan (Paektu) volcano

Bruno Scaillet, Clive Oppenheimer

Reassessment of the sulfur and halogen emissions from the Millennium Eruption of Changbaishan (Paektu) volcano

Bruno Scaillet[1] and Clive Oppenheimer[2]

[1] ISTO, UMR 7327, Université d'Orléans-CNRS-BRGM, 1A rue de la Férollerie, 45071 Orléans cedex 2, FR

[2] Department of Geography, University of Cambridge, Downing Place, Cambridge, CB2 3EN, UK

Abstract

The 946 CE 'Millennium Eruption' of Changbaishan (aka Paektu) volcano ranks among the largest volcanic events of the Common Era. Its fallout represents a widespread precisely-dated marker horizon yet little is known of its environmental impacts. Here, we revisit petrologic constraints on the pre-eruptive conditions of the dominant rhyolitic magma in order to estimate the eruption's volatile budget. We show that silicic reservoirs may lose more than half of their volatile complements prior to eruption and estimate that the Millennium Eruption emitted just 2–7 Tg of sulfur and 5–10 Tg of chlorine to the atmosphere, depending on the accepted eruption magnitude. These values are lower than previous petrologic estimates but consistent with ice core glaciochemistry and tree-ring-based climate reconstructions. We further suggest that any reawakening of Changbaishan / Paektu should be heralded by enhanced CO_2 emissions if driven by basalt intrusion, or by H_2-H_2O-rich and halogen-poor gases if resulting from evolution of a silicic reservoir. Our findings emphasise the importance of robust assessments of pre-eruptive conditions, especially in respect of temperature, when applying petrologic arguments to evaluate outgassing from silicic volcanism.

1. Introduction

Changbaishan / Paektu volcano (hereafter CPV) is renowned for the so-called Millennium Eruption, dated to late 946 CE (likely on or around 2nd November of that year; Oppenheimer et al., 2017). It is one of the few 1st millennium CE eruptions confidently identified in Greenland ice cores (Sun *et al.*, 2014), providing independent means to estimate volatile yields, and enabling synchronisation of cryospheric, marine and terrestrial archives and proxies (e.g., tree-ring based paleoclimate reconstructions) with a precisely-dated event. With an estimated volume of (dense) magma of 24 km^3 (i.e., DRE, corresponding to a magnitude of 6.8; Horn and Schmincke, 2000), it also ranks as one of the largest eruptions in history (Oppenheimer, 2011). Both rhyolite and trachyte magmas were erupted, the former

dispersed widely via a Plinian eruption column (22 km^3 DRE), the latter dispersed and emplaced via pyroclastic density currents and associated co-ignimbrite plumes (2 km^3 DRE). A re-evaluation of the isopach record has suggested downsizing these magnitude estimates by a factor of two (Yang et al., 2021) highlighting the uncertainty in volume calculations but not diminishing the importance of understanding the eruption's potential environmental, climatic and societal impacts from local to hemispheric scales (e.g., Horn and Schmincke, 2000; Xu et al., 2013).

Prior studies of CPV include treatments of stratigraphy (e.g., Wei et al., 2013; Pan et al., 2020; Yang et al., 2022; Zhao et al., 2020); geochemistry of Millennium Eruption deposits (e.g., Zou et al., 2010, 2014); geophysical signals associated with the last unrest episode (e.g., Xu et al., 2012; Wei et al., 2013); and imaging of the deep structure (e.g., Kyong-Song et al., 2016; Hammond et al., 2020). The volatile budget for the Millennium Eruption was first estimated using the 'petrological method' (Horn and Schmincke, 2000), suggesting yields of Cl and F to the atmosphere each exceeding 40 Tg (1 Tg=10^{12}g) and a minimum of 2 Tg of S (i.e., 4 Tg of SO_2). While the role of excess gas in the reservoir (Scaillet et al., 2003) was neglected in these estimates, such a modest syn-eruptive S degassing is not uncommon for silicic eruptions (Westrich and Gerlach, 1991).

More recently, Iacovino et al. (2016) used additional ion microprobe (SIMS) constraints on dissolved volatiles in melt inclusions and trace element behaviour, to argue that the Millennium Eruption could have released up to 45 Tg of S, 20 Tg of Cl, and 58 Tg of F, with more than 90% of S and Cl being sourced in the pre-eruptive excess gas (bubbles). Lower amounts could arise if volatiles were lost during magma residence in the crust as a result of fractionation processes and bubble migration beyond the crystallising melt before eruption. In terms of sulfur, this upper limit would rank the Millennium Eruption only below the Tambora 1815 and Rinjani 1257 eruptions in the Common Era. Such a high estimate, however, is hard to reconcile with the absence of a strong summer cooling in the northern hemisphere as attested by tree-ring proxies (Oppenheimer et al., 2017). Independent evidence for a low S-yield is found in Arctic ice core glaciochemical records, which contain shards of both rhyolite and trachyte matched to the Millennium Eruption (Sun et al., 2014). The corresponding sulfur deposition suggests a low S yield to the stratosphere of order 2 Tg (Sigl et al., 2022).

In the light of these conflicting estimates, we aim here to re-evaluate, from a petrologic perspective, the volatile yields to the atmosphere of the Millennium Eruption. This requires careful assessment of pre-eruptive conditions of the feeding reservoir (depth, temperature, chemical conditions and abundance of any gas phase; e.g., Scaillet et al., 2003; Oppenheimer et al., 2014). We draw on details of the petrology and texture of Millennium Eruption products and apply experimental constraints and knowledge of volatile solubilities, fluid/melt partitioning, and thermodynamic behaviour to determine pre- to syn-eruptive conditions for the dominant rhyolitic magma.

2. Petrological inferences of P-T-fO_2 pre-eruptive conditions of Millennium Eruption rhyolite

Here we use available thermometric estimates, along with phase equilibrium and geochemical data, to constrain the *P-T*-H_2O conditions of magma storage. The majority of the Millennium Eruption deposit consists of crystal-poor (2–3 wt%) alkali and Fe-rich rhyolite (Horn and Schmincke, 2000). The lesser quantity of trachyte erupted is represented in the upper section of the stratigraphy. The erupted rocks define a typical peralkaline trend, with alkali contents increasing with differentiation (i.e., increasing SiO_2 content), but decreasing Al_2O_3 and CaO contents. This corresponds to an increase in magma peralkalinity (NK/A=(Na_2O+K_2O)/Al_2O_3, in moles), the rhyolite end-member classifies as comendite with NK/A=1.2–1.5 (Fig. 1) and FeO=4 wt% (Macdonald, 1974).

The mineralogy of the rhyolite is characterised by alkali feldspar, quartz, clinopyroxene and olivine, accessory minerals being ilmenite, apatite, fluorite and sulphides. The ferromagnesian silicates are close to the Fe endmembers (hedenbergite and fayalite; Zou et al., 2014), reflecting both the extremely low Mg content of the whole rock, and low redox state typical of peralkaline silicic magmas (Scaillet and Macdonald, 2003). Coexistence of almost pure fayalite and quartz, and lack of magnetite imply an oxygen fugacity (fO_2) below that of the Fayalite-Magnetite-Quartz (FMQ) solid buffer (which is 0.7 log units below the reference Ni-NiO buffer, or NNO–0.7). Iacovino et al. (2016) drew on olivine-quartz-ilmenite equilibria to calculate pre-eruptive temperature and fO_2 of 720°C and FMQ–1.2, respectively, the latter consistent with estimates for most peralkaline rhyolites, which lie in the range NNO–1 to NNO–2 (e.g., Di Carlo et al., 2010; White et al., 2009; Romano et al., 2020).

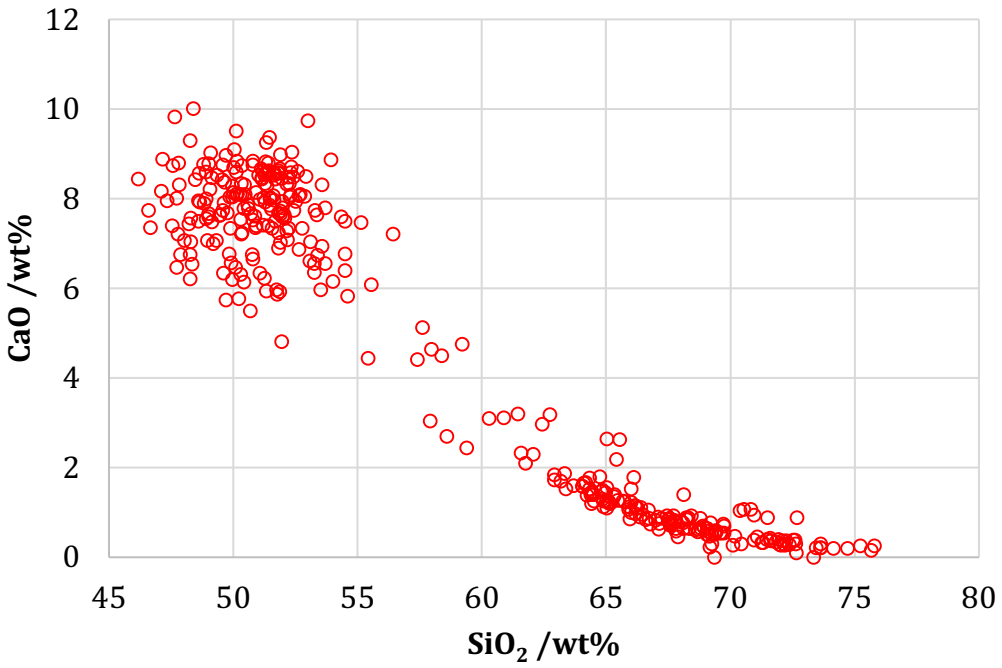

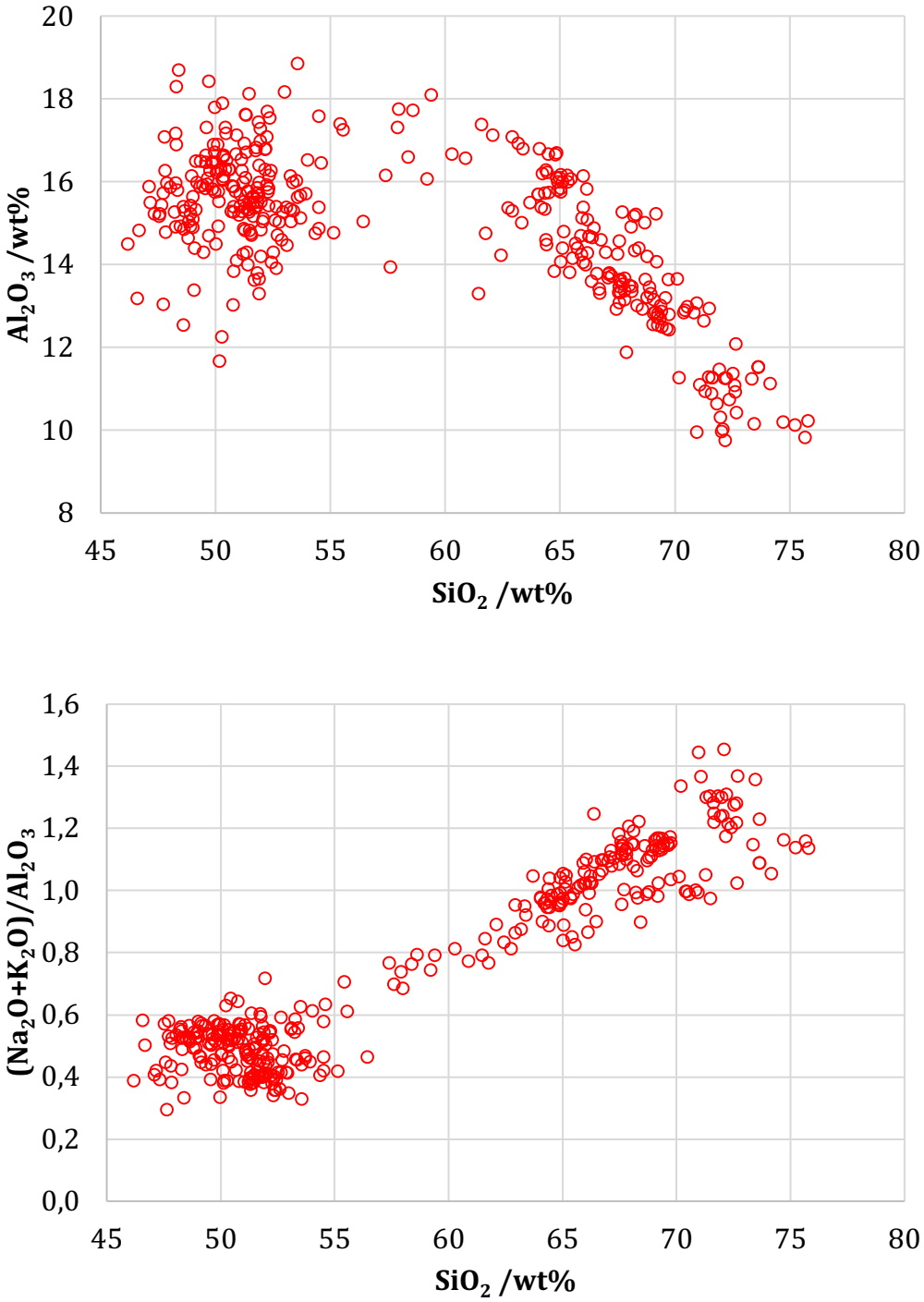

***Figure 1**: Selected major element variations with SiO_2 in CPV rocks. Whole rock data compiled by Zhang et al., 2018.*

The major element compositions of Millennium Eruption rhyolites are close to those of Kenyan peralkaline rhyolites (Table 1), for which detailed phase equilibria have been established under carefully controlled fO_2 conditions (Scaillet and Macdonald, 2001; 2006). The experiments show that alkali feldspar and quartz stabilities are little affected by changes in magma composition, being only slightly depressed by the increase in peralkalinity (Fig. 2).

105 The temperature of crystallisation of both phases steadily increases with decreasing melt
106 water content (H_2O_{melt}) from around 650°C at H_2O saturation (about 5–6 wt% at 150 MPa) up
107 to over 800°C at H_2O_{melt}<2–3 wt%. In all compositions investigated, both phases co-crystallise
108 over a narrow H_2O_{melt} interval.

109 **Table 1.** Whole-rock compositions for the Millennium Eruption comendite compared with
110 comendite from Olkaria (Kenya).

	PKTU-TP*	PEK-26*	PEK-56*	PEK-62*	Kenya**
SiO_2	73.68	74.67	74.66	74.59	74.17
TiO_2	0.225	0.219	0.214	0.21	0.17
Al_2O_3	11.38	10.47	10.51	10.58	10.89
FeO*	4.08	4.24	4.21	4.21	3.98
MnO	0.079	0.078	0.077	0.077	0.06
MgO	0.01	0.04	0.03	0.02	0
CaO	0.28	0.26	0.23	0.22	0.29
Na_2O	5.58	5.56	5.6	5.58	5.81
K_2O	4.69	4.46	4.46	4.51	4.34
P_2O_5	0.008	0.009	0.008	0.007	-
TOTAL	100	100	100	100	100

111 *Analyses from Iacovino *et al*., 2016; **Analysis for sample SMN49 from Scaillet and
112 Macdonald (2001), whose phase equilibrium relationships are shown in Fig. 2b.

113

Analyses of the H_2O_{melt} of feldspar-hosted melt inclusions (MI) in the comendite (Horn and Schmincke, 2000) indicate 4–6 wt% H_2O_{melt}, with an average of 5.2 wt%. The H_2O_{melt} in MI of other phenocrysts is either similar (fayalite) or lower (hedenbergite), the latter case possibly reflecting MI entrapment early in the crystallisation sequence in peralkaline rhyolites (Scaillet and Macdonald, 2001; 2006; Di Carlo et al., 2010), or, more likely, post-eruptive H diffusive loss. Taking an H_2O_{melt} of 5 wt%, along with the constraint of co-precipitation of feldspar and quartz, indicates a pre-eruptive temperature of about 675°C, or even as low as 650°C if the pre-eruptive H_2O_{melt} was closer to 6 wt% (Fig. 2b, comendite SMN49 similar to CPV). Iacovino et al (2016) report lower H_2O contents, between 1 and 4.2 wt%, averaging 2.4 wt%, which would correspond to a pre-eruptive temperature of 800°C, or higher (Fig. 2). The QUILf estimate of 720°C (Iacovino et al., 2016) suggests water contents of 4 wt% (Fig. 2b). In the following, we investigate a pre-eruptive temperature range of 650–700°C which satisfies melt water content constraints determined in MI by both studies. Analyses of CO_2 in melt inclusions yield a maximum of 23 ppm CO_2 in rehomogeneised melt inclusions, most MI lacking detectable CO_2 via SIMS (Iacovino et al., 2016).

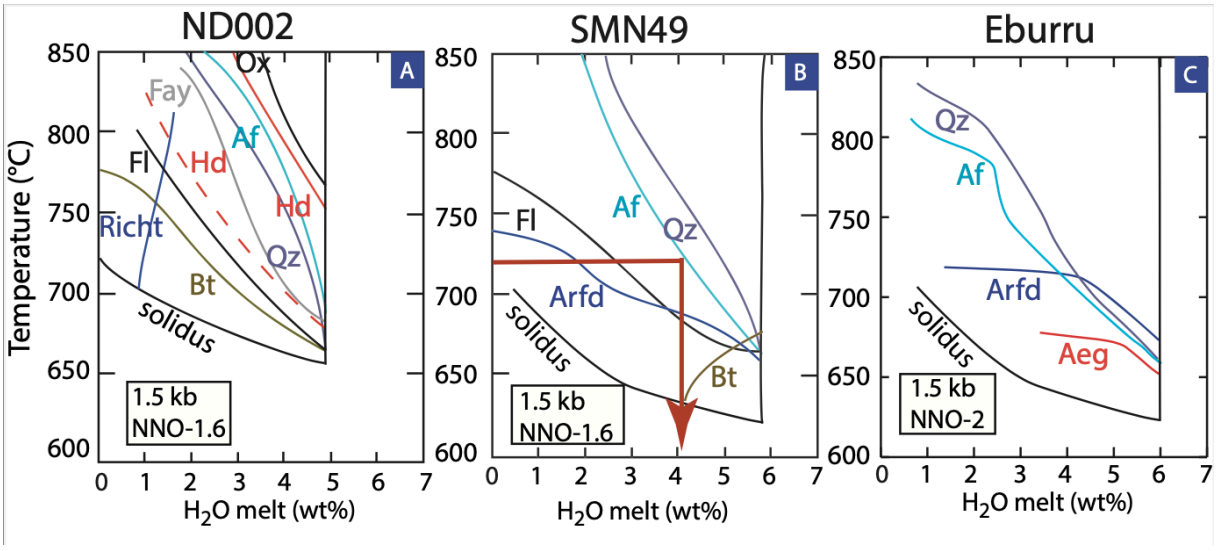

***Figure 2**: Phase relations of three peralkaline rhyolites (Scaillet and Macdonald, 2001; 2006). From left to right, N002-Naivasha, SMN49-Naivasha, and Eburru. Curves are labelled with phase abbreviations as follows: Ox: oxides; Af: alkali feldspar; Fay: fayalite; Hd: hedenbergite; Fl: fluorite; Bt: biotite; Richt: richterite; Arfd: aferdsonite; Aeg: aegirine. In panel B, the red arrow shows the melt H_2O content corresponding to a crystal-poor comendite at about 720°C and saturated in both quartz and feldspar.*

At these conditions, comendite rhyolites are close to their liquidus. For instance, a H_2O-saturated comendite run (H_2O_{melt}=5.8 wt%) at 661°C, 150 MPa, yields magma crystallinities of

1–4 wt% (Scaillet and Macdonald, 2001, 2003), very close to that of Millennium Eruption rhyolites (Horn and Schmincke, 2000). In contrast, a H_2O_{melt} = 3.4 wt% at 730°C and 50 MPa would imply a crystallinity exceeding 15 wt%, while H_2O_{melt} = 3 wt% corresponds to 40 wt% crystals (Scaillet and Macdonald, 2001, 2003), abundances that are not consistent with natural phase proportions. Our temperature estimate is somewhat lower than, but compatible with, that of Zou et al. (2014) who used an alkaki feldspar-glass geothermometer to calculate a temperature of 732°C. Altogether, these temperatures are among the coolest so far estimated for an individual Plinian rhyolitic eruption of this magnitude. For instance, the range is 100–150°C lower that the temperature of the metaluminous, but otherwise comparable, nearly aphyric rhyolite erupted in 2008 from Chaitén volcano (Castro and Dingwell, 2009).

The H_2O_{melt} measured in MI provides a minimum estimate for the depth of the reservoir. Available solubility laws for H_2O in silicic melts (Zhang, 1999) indicate pressures of around 100–120 MPa for H_2O_{melt} of 5–6 wt%. Taking a density of 2700 kg m^{-3} for the crustal rocks above the reservoir, this corresponds to a depth of 4–5 km. We note that this range coincides with that inferred for a magma body from diverse geophysical evidence, including volcano-tectonic earthquake hypocentres recorded during the 2002–2005 crisis, the modelled source of ground deformation (Xu et al., 2012), and seismic velocities in the crust (Hammond et al., 2020). A further pressure estimate comes from the Cl contents of melt inclusions, which cluster around 0.4 wt% (Horn and Schmincke, 2000; Iacovino et al., 2016). This value is similar to that of a brine-saturated comendite melt at about 100 MPa (Métrich and Rutherford, 1992), which suggests that the Millennium Eruption rhyolitic magma, if gas saturated, coexisted with a brine in the reservoir.

The development of a shallow reservoir feeding peralkaline silicic volcanoes appears to be characteristic of this composition of rhyolite magmas (Mahood, 1984), possibly related to extensional tectonics. Note that a pressure of magma storage at 40 MPa, as suggested by Iacovino et al. (2016), would imply Cl contents of about 0.6–0.7 wt% (Métrich and Rutherford, 1992), significantly higher than those observed, either in MI or matrix glass.

3. Amount of excess gas in the Millennium Eruption magma reservoir

Determining the amount of excess gas in the reservoir is critical for petrological assessments of volatile yields to the atmosphere during explosive eruptions (e.g. Scaillet et al., 2003). Previous work has used the behaviour of trace or volatile elements during crystallisation (e.g., Wallace and Gerlach, 1994; Wallace et al., 1995), assuming consanguinity between melt inclusions trapped in crystals (e.g. Papale, 2005). A similar approach has been used by Iacovino et al. (2016), albeit based on the conservation of elements during fractional crystallisation of trachyte to comendite. The tacit assumption underlying the calculations is that volatiles concentrate in the residual liquid until reaching gas-saturation, upon which a free or excess gas phase develops and accumulates as crystallisation proceeds. Using this approach, Iacovino et al. (2016) inferred that the excess gas phase in the reservoir amounted to 3.8 wt% (of the

magma in the reservoir), which would correspond to a volume fraction of 43% were the reservoir at 40 MPa, or, and more reasonably, 23% if at 100 MPa. This assumes (i) that the parental trachyte was not already gas-saturated (in particular without CO_2), and (ii) that no gas loss occurred during its accumulation in the upper reaches of the reservoir prior to eruption.

Here we use an alternative approach drawing on the vesicularity of pumice ejecta from the Millennium Eruption. The terminal porosity of pumices is the sum of pre-existing bubbles in the reservoir and of syn-eruptive degassing. Bubbles grow during decompression, as a result of volatile exsolution and cease expanding when fragmentation occurs in the conduit, at the glass-transition temperature, owing to viscous resistance (e.g., Rust and Cashman, 2004), and when volatile diffusion becomes too slow. At this stage, the residual matrix holds a finite amount of water and other volatiles, such as S, Cl and CO_2. Measurement of those residual volatiles in fresh matrix glass (MG) of Plinian silicic eruptions shows that water content (H_2O_{-MG}) can reach up to 1.5–2.0 wt%. CO_2 in matrix glass (CO_{2-MG}) while less often measured, is generally below 30 ppm (e.g., Newmann et al., 1988; Barnes et al., 2014; Gardner et al., 2017; Giachetti et al., 2020). Sulfur and halogens remain at levels close to pre-eruptive abundances, underscoring their low diffusivities in hydrous rhyolites (e.g., Gerlach et al., 1996).

Compilation of residual water content in matrix glass of explosive rhyolitic eruptions worldwide shows a prominent peak at around 2 wt% (Wadsworth et al., 2022). The origin of water in volcanic glasses is a matter of debate, since secondary hydration is known to occur, especially after prolonged surface exposure (e.g. Giachetti et al., 2015). However, the fact that effusive eruptions clearly define a population with lower H_2O_{-MG} compared with explosive ones, strongly suggests that the peak in H_2O_{-MG} of the latter is largely juvenile in origin. In addition, experimental and numerical simulations (e.g. Hort and Gardner 2000), as well as observations (e.g. Taylor et al., 1983; Newmann et al., 1988), suggest that for the most (early) part, degassing of silicic melts before fragmentation in the upper reaches of the conduit occurs near equilibrium for H_2O and CO_2 and in closed system. For these reasons, we assume that the pressure of fragmentation can be approximated to first order by the sum of partial pressures of the main volatiles, water and CO_2. The latter is given by the use of solubility models of corresponding species (e.g. Blank et al., 1993; Zhang, 1999; Liu et al., 2005). This information, combined with the porosity, enables calculation of the bulk volatile content of magma (melt+bubbles) at fragmentation, neglecting the volatile content of crystals which contribute little to degassing to the atmosphere. We take the density of melt as 2600 kg m^{-3} and approximate the density of gas as that of pure water at the pressure and temperature of fragmentation, assuming perfect gas behaviour, which is reasonable at the low P (<50 MPa) and high T (>650°C) of fragmentation.

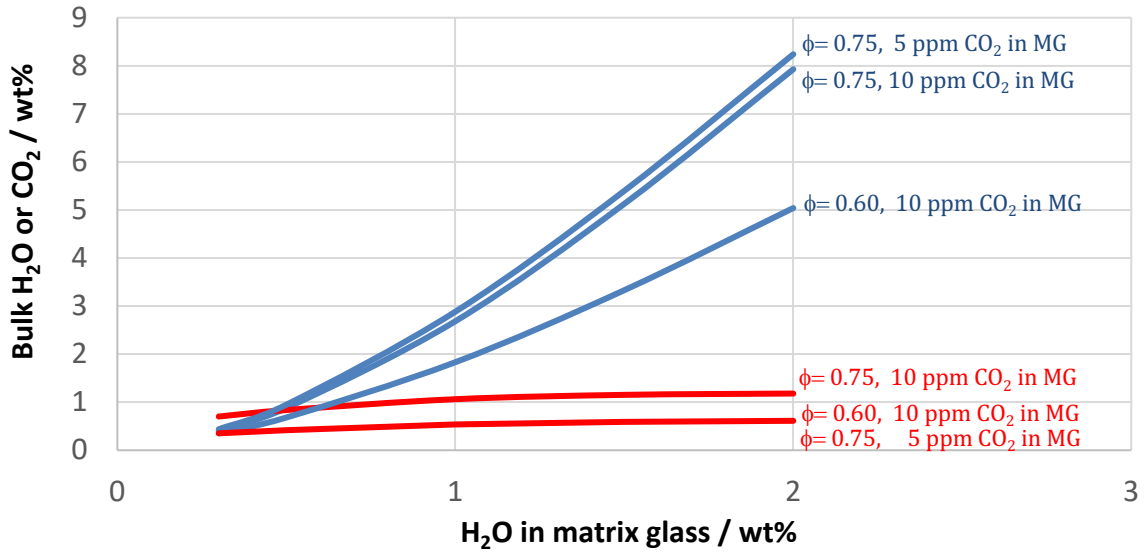

Figure 3*. Relationships between H_2O (blue) and CO_2 (red) contents in matrix glass and bulk volatile contents calculated at fragmentation for different porosities and CO_2 contents in matrix glass ($CO_{2\text{-}MG}$). Note that the curves for the bulk CO_2 at porosities of 0.6 and 0.75 are superimposed.*

Figure 3 illustrates the relationships between H_2O_{melt} in residual glass and bulk H_2O and CO_2 contents at fragmentation, calculated at 700°C for two porosities (ϕ 0.75 and 0.6) and $CO_{2\text{-}MG}$ of 5 and 10 ppm, which is within the range found by, for instance, Newmann et al. (1988), Watkins et al. (2012), Gardner et al. (2017) and Barnes et al. (2014). It shows that CO_2-bulk (melt+bubbles) content ranges from 0.3 to slightly over 1 wt%, whereas H_2O-bulk ranges from about 0.5 wt% to over 8 wt%, depending on porosity.

The next calculation step is carried out by recompressing the magma, keeping constant its bulk volatile content, and maintaining the equilibrium of species fugacities between melt and gas phases, which enables estimation of the amount of H_2O and CO_2 left over in the gas in the reservoir. As an illustration, at fragmentation the basic equation for H_2O is:

$$H_2O_{bulk} = H_2O_{MG} + H_2O_{gas} \qquad (1)$$

In the reservoir, H_2O_{MG} is replaced by H_2O_{melt}, constrained from melt inclusion analyses.

$$H_2O_{bulk} = H_2O_{melt} + H_2O_{gas} \qquad (2)$$

In both cases, the condition of equilibrium requires that:

$$fH_2O_{melt} = fH_2O_{gas} \qquad (3)$$

The same set of equations can be written for CO_2. If there is no CO_2, equations (1) and (2) can be solved directly. Adding CO_2 requires considering the diluting effect of this species on fH_2O,

which is done by varying the amount of excess gas that permits varying the fugacities of H_2O and CO_2 until mass balance and the condition of equilibrium criteria are both satisfied. As a result, there is only one solution of wt% excess gas in the reservoir that reproduces H_2O_{melt} and CO_{2melt} values as inferred from MI, once *P*, *T* and H_2O_{bulk} and CO_{2bulk} are fixed. Given that natural MI have a range of pre-eruptive H_2O and CO_2 contents, this procedure identifies a field of permissible values of wt% excess gas, rather than a unique solution.

The results are shown in Fig. 4, using starting conditions as in Fig. 2. As expected, for any set of final pressure and $CO_{2\text{-}MG}$ conditions, increasing $H_2O_{\text{-}MG}$ leads to an increase in the amount of gas present in the reservoir: the computed amount of free gas at the reservoir *P-T* conditions (700°C and 100–200 MPa) varies between below 1 wt% for a low content of H_2O_{MG} up to over 5 wt% for a H_2O_{MG} of 2 wt% and $CO_{2\text{-}MG}$ at or below 10 ppm. Increasing the $CO_{2\text{-}MG}$ to 30 ppm increases the amount of free gas to over 7 wt%. Decreasing the porosity from 0.75 to 0.60 significantly decreases the amount of gas, by a factor of two to three, depending on $H_2O_{\text{-}MG}$.

The computed curves are also labelled with the corresponding contents of H_2O and CO_2 in the melt. Along each curve, as $H_2O_{\text{-}MG}$ increases, the H_2O_{melt} increases, while the CO_{2melt} decreases. These figures can be directly compared with the concentrations found in melt inclusions, assuming they record reservoir conditions. The work summarised above indicates that pre-eruptive H_2O_{melt} was approximately 4 wt%, with CO_{2melt} barely detectable (≤ 20 ppm), pointing to pre-eruptive gas contents lying on the H_2O-rich side of the diagram. Figure 5 shows the calculations obtained using an average $H_2O_{\text{-}MG}$=1.5 wt%, as determined by Horn and Schmincke (2000), and a porosity of 0.75. It indicates that an amount of free gas slightly above 2 wt% for a reservoir at 100 MPa, 1.5 wt% at 150 MPa, and 1 wt% at 200 MPa, is required to maintain $H_2O_{melt} \geq 4$ wt% and $CO_{2melt} < 30$ ppm (as inferred from MI) at reservoir conditions (Fig. 5). A $CO_{2\text{-}MG}$ of 30 ppm corresponds to higher free gas content in the reservoir (>5 wt%, Fig. 4) but would imply an H_2O_{MG} of at least 2 wt% to yield a pre-eruptive H_2O_{melt} approaching 4 wt%, and the corresponding CO_{2melt} would be much higher (close to 200 ppm) than that measured in MI. We therefore conclude that CO_{2MG} of the Millennium Eruption is likely to be 5 ppm at most, and possibly below 1 ppm (Fig. 4B).

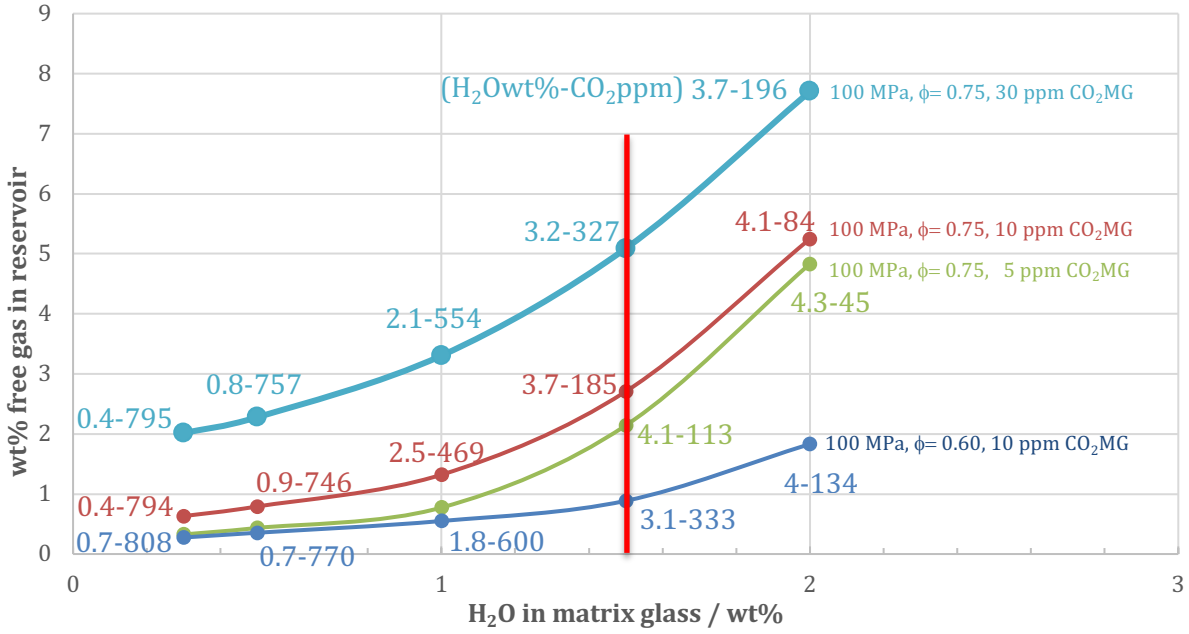

266

267 ***Figure 4***: *Relationships between H_2O in matrix glass at fragmentation and the amount of*
268 *excess gas, calculated at 100 MPa, for different porosities and CO_2 contents of matrix glass, as*
269 *shown on the right of the figure. The vertical red line indicates the average H_2O content of*
270 *Millennium Eruption rhyolite matrix glass as determined by Horn and Schmincke (2000).*
271 *Numbers next to symbols give the corresponding pre-eruptive H_2O_{melt} (wt%) and CO_{2melt} (ppm)*
272 *contents.*

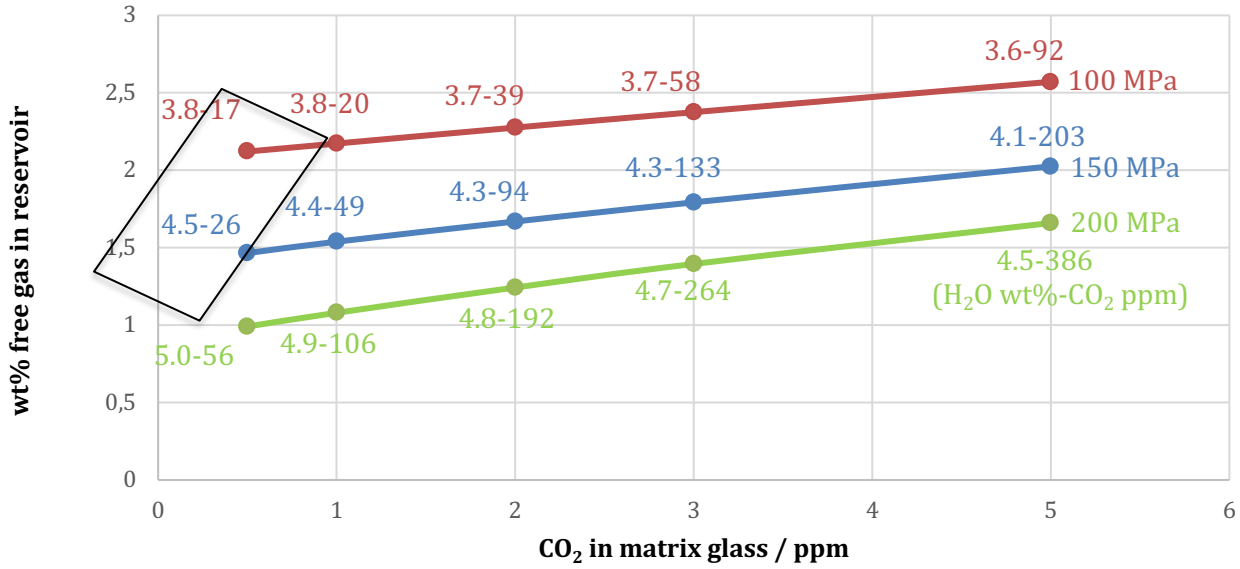

273

274 ***Figure 5***: *Relationships between CO_2 in matrix glass at fragmentation and the amount of*
275 *excess gas, calculated for different reservoir pressures, for a H_2O in matrix glass of 1.5 wt%,*
276 *and a porosity of 0.75. Numbers next to symbols give the corresponding pre-eruptive H_2O_{melt}*

(wt%) and CO_{2melt} (ppm) contents. The oblique rectangle spans the conditions corresponding to H_2O and CO_2 contents determined in melt inclusions.

Computed gas contents with an H_2O_{MG} of 0.3 wt%, as reported by Iacovino et al. 2016, are in all cases lower than 1 wt% (Fig. 4). More importantly, the calculated pre-eruptive H_2O_{melt}, is also < 1 wt%, well below that analysed in melt inclusions, while CO_{2melt} is close to 800 ppm, altogether corresponding with crystal contents exceeding 85 wt% at 700°C, or conditions below solidus at 650°C. This indicates that pumices with low H_2O_{-MG} must have lost a significant amount of dissolved water, either after fallout, or and more likely within the conduit during ascent of the magma. It is possible these fragments experienced more shearing at the flow margins, thereby enhancing permeability (e.g. Okumura et al., 2009; Carrichi et al., 2011; Kushnir et al., 2017), and gas loss. Overall, on the basis of the above calculations, we conclude that the Millennium Eruption reservoir contained 1-2 wt% of free gas (Fig. 5), which had an XH_2O of at least 0.9, and possibly >0.95. Next we address the concentrations of minor volatiles in such a gas.

4. Composition of the gas phase in Millennium Eruption reservoir

The abundance of H_2O of melt inclusions, along with the reduced character of the magma, dictates that H_2 was also abundant in the reservoir (Di Carlo et al., 2010), and that any S present was speciated as H_2S. An unknown is the role of CO_2. However, as stated above, analyses of CO_2 in melt inclusions yield a maximum of 23 ppm CO_2 (Iacovino et al., 2016). This is in agreement with other peralkaline centres (e.g., Neave et al., 2012), where CO_2 is present in low amounts or below the detection level (about 20–100 ppm). This most probably reflects the protracted fractionation needed to produce peralkaline silicic derivatives from more mafic parents, during which most of the CO_2 is lost from the plumbing system before the rhyolites are produced (Di Carlo et al., 2010). A five-fold increase, between trachyte and rhyolite, is observed in incompatible trace elements such as Nb, Sn, Zr, U, Th, or W in peralkaline series (Civetta et al., 1998 ; Macdonald et al., 2008), as illustrated for Zr and Nb in CPV whole rock analyses (Fig. 6). This indicates that comendite production requires about 80 wt% crystallisation of parental trachyte magma, as inferred also by Iacovino et al. (2016). We conclude therefore that, even if the mafic parental magmas of Millennium Eruption rhyolites held some CO_2 during early stages of fractionation, its abundance was negligible in the rhyolitic reservoir.

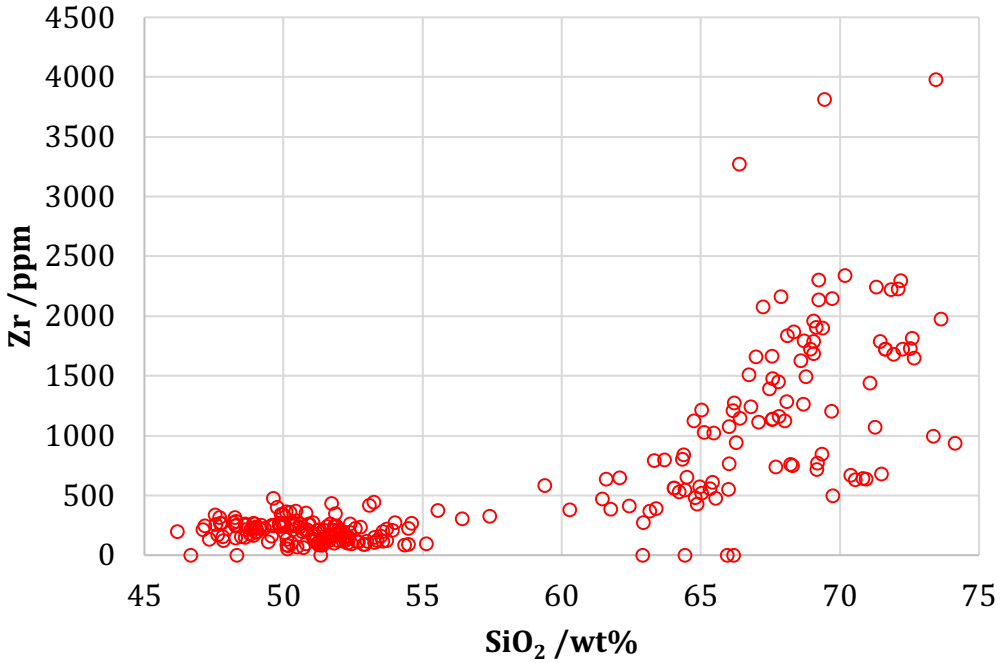

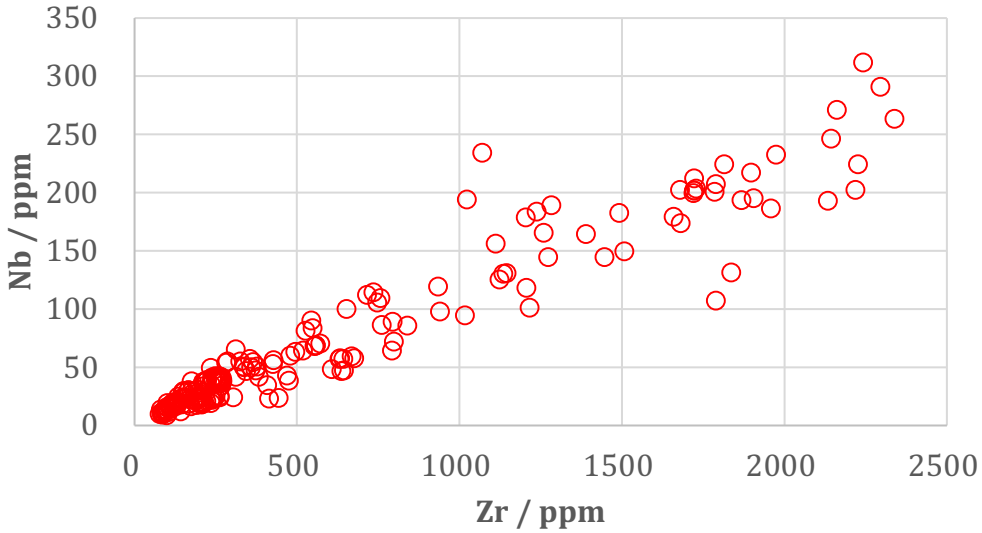

***Figure 6**. Evolution of Zr during fractionation from basalt to trachyte to comendite at CPV. Whole rock data compiled by Zhang et al., 2018. Nb is taken to illustrate the highly incompatible behaviour of a trace element during crystallisation of basalt to trachyte (about 65 wt% SiO_2, 70 ppm Nb and 500 ppm Zr) to comendite.*

4.1. The case for sulfur

The case for sulfur is analogous to that for halogens, albeit for different reasons. Experiments have shown that peralkalinity increases sulfur solubility in silicic melts (Scaillet and Macdonald, 2006b). As a result, S behaves broadly as an incompatible element in mafic to silicic fractionation producing peralkaline magmas, at least to the point of gas saturation. The gas/melt partition coefficient of S (D_S) in comendite melts in the fO_2 range NNO–1 to NNO–2

(Scaillet and Macdonald, 2006) is 200–300 at 800°C. A decrease of 100°C decreases D_S by a factor of ten in metaluminous rhyolites (Scaillet et al., 1998), hence in the temperature range 650–700°C we infer a Ds of about 20–30, similar to that established for reduced metaluminous silicic magmas owing to the expanded stability field of pyrrhotite, which locks up the majority of available S (Scaillet et al., 1998). 80% of MI and MG reported by Horn and Schmincke (2000) had S contents below the detection limit (250 ppm), while MI analyses of Iacovino et al. (2016) indicated an average S content of 110±3 ppm, altogether suggesting a maximum S content of about 0.2–0.3 wt% for the average pre-eruption gas. This is about 10–20 times less than that inferred for the 1991 Mt. Pinatubo dacite (2–6 wt% S, Scaillet et al., 1998, 2003). Considering the S content of 455±90 ppm in the 20% MI where S could be detected would suggest an S content of the gas of less than 0.4 wt%.

Given that the above figure comes from an extrapolation beyond the calibrated range, we also constrain the S content of the gas via a thermodynamic approach. We use the following equilibrium between pyrrhotite (FeS_{Po}) and Fe^{2+} in the liquid (FeO_{liq}):

$$FeS_{po} + ½\ O_2 \leftarrow\!\!-\!\!\rightarrow FeO_{liq} + ½\ S_2 \qquad (4)$$

whose equilibrium constant is:

$$K_1 = aFeO_{liq} * (fS_2)^{1/2} / aFeS_{po} * (fO_2)^{1/2} \qquad (5)$$

We take advantage of the fact that pyrrhotite is a common sulphide in reduced rhyolites (e.g. Whitney, 1984), including in the Millennium Eruption comendite (Iacovino et al., 2016). Thermodynamic data (e.g. Robie and Hemingway, 1995; Barin, 1995) allow calculation of K_1. We take the Gibbs free energy of formation of FeO_{liq} and FeS_{Po} and heat capacities from Gaillard et al. (2003) and Barin (1995), respectively; and the molar volumes of solids from Robie and Hemingway (1995) and liquid FeO from Lange (1994). The fO_2 value is that determined by Iacovino et al. (2016). The main unknown in this approach comes from the term $aFeO_{liq}$. For the Millennium Eruption comendite we build upon the fact that the rhyolite is saturated with an Fe-rich olivine (fayalite) and quartz so that the following equilibrium holds:

$$Fe_2SiO_{4\text{-}Ol} \leftarrow\!\!-\!\!\rightarrow 2\ FeO_{liq} + SiO_{2\text{-}qz} \qquad (6)$$

whose equilibrium constant is given by:

$$K_2 = (aFeO_{liq})^2 * aSiO_{2\text{-}qz} / aFe_2SiO_{4\text{-}Ol} \qquad (7)$$

The Gibbs free energies of formation of fayalite and quartz are taken from Barin (1995) which along with that for FeO_{liq} from Gaillard et al. (2003), and the partial molar volume of FeOliq from Lange (1994), allow us to compute K_2 (using standard states for solids and liquids at given *P* and *T*). To calculate $aFeO_{liq}$, we first assume that quartz is pure ($aSiO_2$=1). For olivine, the data of Zou et al (2014) show that Ol is nearly pure fayalite (XFe_2SiO_4 = 0.98), which, with the

model of O'Neill et al. (2003), implies an activity coefficient close to 1 (hence aFay=XFay). Solving equation (7) for a P =100 MPa and T=700°C gives an $aFeO_{liq}$ =0.031 (0.021 for 650°C). Rearranging (5), we have:

$$fS_2 = (aFeS_{po} * (fO_2)^{1/2*} K_1 / aFeO_{liq})^2 \quad (8)$$

and using the activity for FeO_{liq}, the fO_2 as determined by Iacovino et al (2016) and the K_1 value as explained previously, yields an $fS_2 = 1.9 \times 10^{-7}$ bar, for $Fe_{0.877}S$ pyrrhotite (Barin, 1995) which corresponds to $aFeS_{po}$ = 0.37 (Toulmin and Barton, 1964). At 650°C, the fS_2 is 4×10^{-8} bar (note that the lack of pyrrhotite in rhyolite would imply that calculated fS_2 are maxima).

The next step is to calculate the corresponding fugacity of H_2S (fH_2S), the dominant S-bearing species in reduced magmas. To do so we use the following equilibria:

$$H_2 + ½\ S_2 = H_2S \quad (9)$$

and

$$H_2 + ½\ O_2 = H_2O \quad (10)$$

Equilibrium (10) allows calculation of fH_2, knowing fO_2 (Iacovino et al., 2016) and fH_2O, the latter being given by thermodynamic model of Zhang (1999), which relates water content of the melt (4 wt%) to its fugacity. Use of calculated fH_2 and fS_2 and standard thermodynamic data for (9), yields an fH_2S of 0.28 MPa. The conversion of fH_2S into XH_2S_{gas} (mole fraction of H_2S in the gas) is achieved with the following standard relationship:

$$XH_2S_{gas} = fH_2S / \gamma H_2S * P_{tot} \quad (11)$$

Here, P_{tot} is total pressure (=100 MPa), γH_2S (=1.05) is the fugacity coefficient of H_2S gas species which is here calculated using a modified Redlich-Kwong equation of state (MRK-EOS), using parameters given by Holloway (1987). The resulting XH_2S_{gas}=0.0023, which corresponds to an S content of 0.4 wt%, lies at the upper end of the range inferred from extrapolating the experiments of Scaillet and Macdonald (2006) to lower temperatures, but is almost four times less than the estimate (1.8 wt%) of Iacovino et al. (2016). Performing the above set of calculations at a pre-eruptive temperature of 650°C would further decrease the S content of the pre-eruptive gas to 0.3 wt%. These figures yield a partition coefficient of S between gas and melt of 30–40 (for comendite rhyolite at 650–700°C and FMQ–1.2).

The above constraints on gas phase composition represent a rigorous framework for interpreting geochemical signals associated with unrest (see below), but also enable evaluation of the volatile yields to the atmosphere of the Millennium Eruption. The elevated H_2O_{melt} of Millennium Eruption rhyolites indicates an H_2O-rich environment, promoting gas saturation, as suggested also by Cl systematics. Since the 1980 El Chichón eruption (Luhr et al., 1984), excess gas has been called upon to resolve the so-called 'excess sulfur' problem

especially in arc settings (e.g. Westrich and Gerlach, 1991; Métrich and Mandeville, 2010), for which remote sensing methods detect 10–20 times more S than that which could have been supplied by syn-eruptive melt degassing.

Previous geochemical modelling has shown that silicic reservoirs may hold up to 5–6 wt% gas at their apices at around 150–200 MPa (Wallace et al., 1999), corresponding to 20–25 vol% at this pressure. Higher gas contents seem to be precluded by the fact that bubbles start to form an interconnected network allowing continuous gas escape from the reservoir beyond this threshold (Wallace, 2001; 2005). Storage at low pressure, around 100 MPa such as in the case of the Millennium Eruption rhyolite, significantly decreases water density relative to the common storage pressure of 200 MPa observed in arc settings (0.3 g/cm^3 vs 0.5 g/cm^3, respectively) which should reduce the maximum gas retainable in the reservoir.

Neglecting crystallinity, the atmospheric S (or Cl) yield in Tg of an eruption emitting A km^3 (DRE) of magma with a density of ρ kg/m^3, stored in a reservoir with B wt% gas which has C wt% S (or Cl) is given by:

$$\text{S yield (Tg)} = 10^{-4} \times A \times \rho \times B \times C \qquad (10)$$

Assuming that the Millennium Eruption reservoir contained 1–2 wt% gas with 0.3–0.4 wt% S, gives a sulfur yield to the atmosphere of 1.7–4.5 Tg. To this amount should be added 2.6 Tg of S due to syn-eruptive degassing of comendite, and 0.2 Tg of S from the minor trachyte component (calculated assuming syn-eruptive degassing of 2 km^3 of trachyte magma having lost 42 ppm S (Iacovino et al. 2016), which gives a total amount of S ranging between 4.5 and 7.3 Tg, or half as much (2.2–3.6 Tg) using the eruption magnitude of Yang et al. (2021). The lower figures are 2–4 times lower than that associated with the 1991 eruption of Mt. Pinatubo (10 Tg S, Bluth et al., 1992). Our lower estimate is consistent with the evidence for a comparatively low S yield estimated from polar ice records (Sigl et al., 2015; 2022).

The significantly higher S yield (up to 42 Tg) calculated by Iacovino et al. (2016) derive essentially from assuming conservation of volatile elements during fractionation of trachyte to comendite, which led them to compute an excess gas phase of 3.8 wt%. Our analysis shows, however, that this gas phase amounts to 1-2 wt%, suggesting that at least half of it may be lost during crustal residence of silicic magmas prior to eruption. The calculated bulk S content of comendite magma ranges between 150 and 190 ppm, depending on the amount of fluid (1 and 2 wt%, respectively). This is less than that which could have been delivered by the parental trachyte (which has 197 ppm S, Iacovino et al., 2016): assuming that S was entirely passed to the comendite after about 80 wt% of trachyte fractionation, there would be 985 ppm of S in comendite. The 4–5 fold decrease in S amount of the erupted comendite magma reflects loss of this element during fractionation, either through sequestration in sulfides (pyrrhotite, molybdenite) as shown by Iacovino et al. (2016), or owing to pre-eruptive gas loss from the reservoir.

While the precursor magmas were volatile-rich, in particular in H_2O and halogens, their reduced character, low temperature, shallow storage pressure, and the topology of Cl bearing fluids, all combined to inhibit extensive outgassing of atmospherically-relevant species. Our results emphasise the importance of estimating the outgassing from past eruptions on a case by case basis.

4.2. The case for chlorine

As with many other peralkaline rhyolites, those of CPV are quite halogen-rich compared with their metaluminous counterparts, suggesting the possibility of high syn-eruptive emissions of halogens to the atmosphere. The possibility that the magma was brine-saturated in the reservoir enables a first-order calculation of the Cl content of the gas phase. The H_2O-NaCl system is characterised by a solvus at pressures below 200 MPa (Bodnard et al., 1985) where the H_2O-rich gas coexists with a Cl-rich phase (brine). At 700°C and 100 MPa, i.e., conditions approaching those inferred for the Millennium Eruption comendite, the gas phase is topologically constrained to have no more than 1–2 wt% Cl (Bodnard et al., 1985). At this temperature, the crest of the NaCl-H_2O solvus is at 120 MPa, beyond which NaCl and H_2O are fully miscible, though the presence of K and Fe will expand the solvus towards higher pressure (Liebscher, 2007).

Two additional factors indicate that the contents of Cl in the gas phase estimated above are upper bounds. First, the solubility of Cl of silicate melts at brine saturation increases with decreasing pressure, notably in peralkaline rhyolites (Métrich and Rutherford, 1992), which requires that during ascent, degassing at equilibrium must produce increasingly Cl-poor gases. Secondly, the limbs of the H_2O-NaCl solvus strongly expand as pressure decreases, such that the gas becomes more H_2O-rich during ascent: for instance, at 50 MPa, the Cl content of the hydrous gas drops by more than one order of magnitude relative to that at 100 MPa.

Although previous work (Horn and Schmincke, 2000) evaluated halogen yields by comparing MG versus MI abundances, a close inspection reveals that Cl values in both MG and MI of Plinian fallouts are essentially the same in light of uncertainties (0.41±0.06 wt% *vs* 0.44±0.11 wt%, respectively). This points to minimal syn-eruptive degassing, consistent with our topological argument. This conclusion is also borne out by the data reported by Iacovino et al (2016) which show that Cl in MG is even slightly higher than in MI, though still within error of it (4166±225 ppm vs 3974±215 ppm, respectively). According to Iacovino et al. (2016), almost all (> 95 wt.%) Cl (and S) expelled by the magma resided in pre-existing fluid, stressing the importance of a correct estimate of the amount of that phase in the reservoir.

Though not analysed in CPV rocks, the study of Br in evolved magmas (Bureau and Métrich, 2003) shows this element to be essentially undegassed during eruption of peralkaline silicic melts (Br contents in melt inclusion and matrix glass being identical). Hence, despite their halogen-rich character, alkali-rich silicic magmas stored at shallow levels may not be correspondingly large emitters of halogens to the atmosphere on eruption. For a magma

463 volume of 22 km^3 (DRE), an excess gas of 2 wt%, and a conservative Cl content of gas of 1 wt%,
464 about 10 Tg Cl would have been lofted to the atmosphere (see below for the details of
465 calculation), or half this amount if the eruption magnitude is halved (Yang et al., 2021). This
466 amount of Cl is half that of Iacovino et al. (2016), essentially reflecting that our estimate of
467 free gas in the reservoir is half the value of 3.8 wt.% of Iacovino et al. (2016).

468

469 ## 5. Considerations on future unrest of CPV

470 Radiometric dating (Wei et al., 2007) indicates that volcanism in the CPV area began around 4
471 Ma ago, with emplacement of basalts forming large shields and plateaus. This was followed
472 by a cone construction period (<1 Ma) dominated by eruption of trachytes, and then by the
473 ignimbrite stage as typified by the Millennium Eruption, which characterises activity for the
474 last several thousands of years. The overall temporal evolution of magma composition
475 indicates that the temperature of the plumbing system has progressively declined, since
476 abundant trachyte-comendite generation requires cooling of the parental basaltic magmas.

477 Comendites are dominantly produced by crystal fractionation of alkali basalt, via a trachyte
478 stage (Macdonald et al., 2008; 2021). The 10–30 km^3 of near aphyric comendite discharged
479 with the Millennium Eruption implies efficient separation from a trachytic magma mush at
480 depth, whose volume should be approximately 50–100 km^3, on the basis of the fivefold
481 increase in incompatible elements between trachyte and rhyolite (Fig. 5). Mush compaction
482 has been advocated as one mechanism for production of crystal-poor rhyolites (Bachmann
483 and Bergantz, 2004). The area of the caldera is about 36 km^3, which we take as the minimum
484 planimetric area of the underlying reservoir (Wei et al., 2013). This implies that the thickness
485 of the segregated layer of melt was 600–700 m. Considering its volume, the thickness of the
486 underlying trachyte magma body is probably of order of a few kilometres.

487 Owing to its elevated crystallinity (70–80%) by the time of comendite production, heat losses
488 from such a body would be mostly conductive. Assuming a half thickness of 2 km implies a
489 conductive cooling time of about 160 ka. A simple application of the model of McKenzie
490 (1984), shows that the corresponding timescale of melt segregation of a 4 km compacting
491 mush pile with 20–30 vol % liquid, varies from 90 ka (for a melt viscosity of 10^4 Pa s) to 530 ka
492 (for a viscosity of 10^5 Pa s), with corresponding thicknesses of the segregated melt layer
493 reaching 500 and 750 m, respectively. It is not clear, however, that compaction readily
494 operates in silicic reservoirs (see Holness, 2018), and in fact the mechanisms of melt extraction
495 from silicic to intermediate mushes remain obscure (e.g., Bachmann and Huber, 2019).

496 We note that the cooling and segregation timescales given above are comparable, though the
497 latter are not as fast as diffusion chronometry suggests, including for magmatic reservoirs of
498 dimension comparable to that of CPV, for which melt extraction timescales of decades to
499 months have been inferred (e.g., Santorini; Druitt et al., 2012). The viscosity of natural (i.e.,

iron-rich) peralkaline rhyolites is poorly known, but experiments on model compositions (i.e., Fe-free) indicate that peralkalinity dramatically decreases silicic melt viscosities (Dingwell et al., 1998). Based on previous assessment of rhyolite viscosities worldwide (Scaillet et al., 1998), which indicate a range from 10^4 to 10^5 Pa s, we suggest that CPV rhyolite magmas have a viscosity close to 10^4 Pa s. For this value, the calculated timescale is compatible with residence timescales inferred from zircon geochronology for the Millennium Eruption rhyolite, which range up to 10 ka prior to eruption (Zou et al., 2010; 2014), indicating a long-lived rhyolitic magma body, which has been stagnating for several thousand or tens of thousands of years. Such a protracted residence may have favoured volatile escape from the roof of the reservoir.

The large silicic reservoir has clearly acted as a trap for any rising basaltic magmas during the latter period of CPV's evolution. While very little is known about activity of CPV since the Millennium Eruption, there is some evidence that it has continued to erupt rhyolites (Wei et al., 2013). If this is correct, it would suggest sustained mobility of the silicic reservoir, and hence the potential for future rhyolitic eruptions. An episode of increased seismicity and deformation, and compositional changes in hydrothermal fluids between 2002 and 2005 was interpreted as magmatic unrest (Hahm et al., 2007; Xu et al., 2012). Our analysis shows that fluids escaping from such an associated reservoir will be H_2O-, H_2- and H_2S-rich, with comparatively minor halogens. Remobilisation of such a body would not be expected to result in an increase in diffusive CO_2 flux on the volcano. In the case that there is a significant increase in CO_2 at the surface, this might suggest arrival of mafic magma (basalt or trachyte) in the upper reaches of the plumbing system, and the possible re-opening (or by-passing) of the barrier imposed by the silicic system to more mafic eruptions.

6. Acknowledgements

This work has been supported by Labex Voltaire ANR-10-LABX-100-01 and Equipex PLANEX ANR-11-EQPX-0036 projects. We thank Tom Sisson and Nicole Métrich for their detailed reviews that helped to improve the manuscript and Tobias Fischer for his careful editorial handling.

7. References

Bachmann, O., & Bergantz, G. W. (2004). On the origin of crystal-poor rhyolites: extracted from batholithic crystal mushes. *Journal of Petrology*, *45*(8), 1565-1582.

Bachmann, O., & Huber, C. (2019). The inner workings of crustal distillation columns; the physical mechanisms and rates controlling phase separation in silicic magma reservoirs. *Journal of Petrology*, *60*(1), 3-18.

Barin, I. (1995). Thermodynamic data of pure substances, VCH verlagsgeserschaft mbH.

Barnes, J. D., Prather, T. J., Cisneros, M., Befus, K., Gardner, J. E., & Larson, T. E. (2014). Stable chlorine isotope behavior during volcanic degassing of H_2O and CO_2 at Mono Craters, CA. *Bulletin of Volcanology*, *76*(3), 1-13.

Blank, J. G., Stolper, E. M., & Carroll, M. R. (1993). Solubilities of carbon dioxide and water in rhyolitic melt at 850 C and 750 bars. *Earth and Planetary Science Letters*, *119*(1-2), 27-36.

Bluth, G. J., Doiron, S. D., Schnetzler, C. C., Krueger, A. J., & Walter, L. S. (1992). Global tracking of the SO_2 clouds from the June, 1991 Mount Pinatubo eruptions. *Geophysical Research Letters*, *19*(2), 151-154.

Bodnar, R. J., Burnham, C. W., & Sterner, S. M. (1985). Synthetic fluid inclusions in natural quartz. III. Determination of phase equilibrium properties in the system H_2O-NaCl to 1000 C and 1500 bars. *Geochimica et Cosmochimica Acta*, *49*(9), 1861-1873.

Caricchi, L., Pommier, A., Pistone, M., Castro, J., Burgisser, A., & Perugini, D. (2011). Strain-induced magma degassing: insights from simple-shear experiments on bubble bearing melts. *Bulletin of volcanology*, *73*(9), 1245-1257.

Castro, J. M., & Dingwell, D. B. (2009). Rapid ascent of rhyolitic magma at Chaitén volcano, Chile. *Nature*, *461*(7265), 780-783.

Civetta, L., Massimo, D. A., Orsi, G., & Tilton, G. R. (1998). The geochemistry of volcanic rocks from Pantelleria Island, Sicily Channel: petrogenesis and characteristics of the mantle source region. *Journal of Petrology*, *39*(8), 1453-1491.

Di Carlo, I., Rotolo, S. G., Scaillet, B., Buccheri, V., & Pichavant, M. (2010). Phase equilibrium constraints on pre-eruptive conditions of recent felsic explosive volcanism at Pantelleria Island, Italy. *Journal of Petrology*, *51*(11), 2245-2276.

Dingwell, D. B., Hess, K. U., & Romano, C. (1998). Extremely fluid behavior of hydrous peralkaline rhyolites. *Earth and planetary science letters*, *158*(1), 31-38.

Druitt, T. H., Costa, F., Deloule, E., Dungan, M., & Scaillet, B. (2012). Decadal to monthly timescales of magma transfer and reservoir growth at a caldera volcano. *Nature*, *482*(7383), 77-80.

Gaillard, F., Pichavant, M., & Scaillet, B. (2003). Experimental determination of activities of FeO and Fe_2O_3 components in hydrous silicic melts under oxidizing conditions. *Geochimica et Cosmochimica Acta*, *67*(22), 4389-4409.

Gardner, J. E., Llewellin, E. W., Watkins, J. M., & Befus, K. S. (2017). Formation of obsidian pyroclasts by sintering of ash particles in the volcanic conduit. *Earth and Planetary Science Letters*, *459*, 252-263.

571 Gerlach, T. M., Westrich, H. R., & Symonds, R. B. (1996). Preeruption vapor in magma of the
572 climactic Mount Pinatubo eruption: Source of the giant stratospheric sulfur dioxide cloud.
573 *Fire and mud: eruptions and lahars of Mount Pinatubo, Philippines*, *415*, 33.

574 Giachetti, T., Gonnermann, H. M., Gardner, J. E., Shea, T., & Gouldstone, A. (2015).
575 Discriminating secondary from magmatic water in rhyolitic matrix-glass of volcanic pyroclasts
576 using thermogravimetric analysis. *Geochimica et Cosmochimica Acta*, *148*, 457-476.

577 Giachetti, T., Hudak, M. R., Shea, T., Bindeman, I. N., & Hoxsie, E. C. (2020). D/H ratios and
578 H_2O contents record degassing and rehydration history of rhyolitic magma and pyroclasts.
579 *Earth and Planetary Science Letters*, *530*, 115909.

580 Hahm, D., Hilton, D. R., Cho, M., Wei, H., & Kim, K. R. (2008). Geothermal He and CO_2
581 variations at Changbaishan intra-plate volcano (NE China) and the nature of the sub-
582 continental lithospheric mantle. *Geophysical Research Letters*, *35*(22).

583 Hammond, James OS, Jian-Ping Wu, Kyong-Song Ri, Wei Wei, Jong-Nam Yu, and Clive
584 Oppenheimer (2020) Distribution of partial melt beneath Changbaishan/Paektu Volcano,
585 China/democratic people's Republic of Korea." *Geochemistry, Geophysics, Geosystems* 21,
586 no. 1: e2019GC008461.

587 Holness, M. B. (2018). Melt segregation from silicic crystal mushes: a critical appraisal of
588 possible mechanisms and their microstructural record. *Contributions to Mineralogy and*
589 *Petrology*, *173*(6), 48.
590
591 Holloway, J. R. (1987). Igneous fluids. In *Thermodynamic Modeling of Geologic Materials*:
592 *Minerals, Fluids and Melts*, Rev Miner.17, 211-232.

593 Horn, S., & Schmincke, H. U. (2000). Volatile emission during the eruption of Baitoushan
594 Volcano (China/North Korea) ca. 969 AD. *Bulletin of Volcanology*, *61*(8), 537-555.

595 Hort, M., & Gardner, J. (2000). Constraints on cooling and degassing of pumice during Plinian
596 volcanic eruptions based on model calculations. *Journal of Geophysical Research: Solid Earth*,
597 *105*(B11), 25981-26001.

598 Kushnir, A. R., Martel, C., Champallier, R., & Arbaret, L. (2017). In situ confirmation of
599 permeability development in shearing bubble-bearing melts and implications for volcanic
600 outgassing. *Earth and Planetary Science Letters*, *458*, 315-326.

601 Kyong-Song, R., Hammond, J.O., Chol-Nam, K., Hyok, K., Yong-Gun, Y., Gil-Jong, P., Chong-
602 Song, R., Oppenheimer, C., Liu, K.W., Iacovino, K. and Kum-Ran, R., 2016. Evidence for partial
603 melt in the crust beneath Mt. Paektu (Changbaishan), Democratic People's Republic of Korea
604 and China. *Science Advances*, *2*(4), p.e1501513.

Liebscher, A. (2007). Experimental studies in model fluid systems. *Reviews in Mineralogy and Geochemistry*, *65*(1), 15-47.

Liu, Y., Zhang, Y., & Behrens, H. (2005). Solubility of H_2O in rhyolitic melts at low pressures and a new empirical model for mixed H_2O–CO_2 solubility in rhyolitic melts. *Journal of Volcanology and Geothermal Research*, *143*(1-3), 219-235.

Macdonald, R. (1974). Nomenclature and petrochemistry of the peralkaline oversaturated extrusive rocks. *Bulletin volcanologique*, *38*, 498-516.

Macdonald, R., Belkin, H. E., Fitton, J. G., Rogers, N. W., Nejbert, K., Tindle, A. G., & Marshall, A. S. (2008). The roles of fractional crystallization, magma mixing, crystal mush remobilization and volatile–melt interactions in the genesis of a young basalt–peralkaline rhyolite suite, the Greater Olkaria Volcanic Complex, Kenya Rift Valley. *Journal of Petrology*, *49*(8), 1515-1547.

Macdonald, R., White, J. C., & Belkin, H. E. (2021). Peralkaline silicic extrusive rocks: magma genesis, evolution, plumbing systems and eruption. *Comptes Rendus. Géoscience*, *353*(S2), 7-59.

Machida, H., Moriwaki, H., & Zhao, D. C. (1990). The recent major eruption of Changbai Volcano and its environmental effects. *Geograph. Rep. Tokyo Metro. Univ.* 25, 1-20

Mahood, G. A. (1984). Pyroclastic rocks and calderas associated with strongly peralkaline magmatism. *Journal of Geophysical Research: Solid Earth (1978–2012)*, *89*(B10), 8540-8552.

McKenzie, D. A. N. (1984). The generation and compaction of partially molten rock. *Journal of Petrology*, *25*(3), 713-765.

Metrich, N., & Rutherford, M. J. (1992). Experimental study of chlorine behavior in hydrous silicic melts. *Geochimica et Cosmochimica Acta*, *56*(2), 607-616.

Métrich, N., & Mandeville, C.W. (2010). Sulfur in magmas. *Elements* 6.2: 81-86.

Neave, D. A., Fabbro, G., Herd, R. A., Petrone, C. M., & Edmonds, M. (2012). Melting, differentiation and degassing at the Pantelleria volcano, Italy. *Journal of Petrology*, egr074.

Newman, S., Epstein, S., & Stolper, E. (1988). Water, carbon dioxide, and hydrogen isotopes in glasses from the ca. 1340 AD eruption of the Mono Craters, California: Constraints on degassing phenomena and initial volatile content. *Journal of Volcanology and Geothermal Research*, *35*(1-2), 75-96.

637 Okumura, S., Nakamura, M., Takeuchi, S., Tsuchiyama, A., Nakano, T., & Uesugi, K. (2009).
638 Magma deformation may induce non-explosive volcanism via degassing through bubble
639 networks. *Earth and Planetary Science Letters*, *281*(3-4), 267-274.

640 O'Neill, H. S. C., Pownceby, M. I., & McCammon, C. A. (2003). The magnesiowüstite: iron
641 equilibrium and its implications for the activity-composition relations of $(Mg, Fe)_2SiO_4$ olivine
642 solid solutions. *Contributions to Mineralogy and Petrology*, *146*(3), 308-325.

643 Oppenheimer, C., Fischer, T. P., & Scaillet, B. (2014). Volcanic degassing: process and impact.
644 In *Treatise on Geochemistry (Second Edition) Vol. 4* (pp. 111-179).

645 Oppenheimer, C., Wacker, L., Xu, J., Galván, J.D., Stoffel, M., Guillet, S., Corona, C., Sigl, M.,
646 Di Cosmo, N., Hajdas, I. and Pan, B., 2017. Multi-proxy dating the 'Millennium Eruption' of
647 Changbaishan to late 946 CE. *Quaternary Science Reviews*, *158*, 164-171.

648 Pan, Bo, Shanaka L. de Silva, Jiandong Xu, Songjun Liu, and Dan Xu. "Late Pleistocene to
649 present day eruptive history of the Changbaishan-Tianchi Volcano, China/DPRK: New field,
650 geochronological and chemical constraints." *Journal of Volcanology and Geothermal*
651 *Research* 399 (2020): 106870.

652 Papale, P. (2005). Determination of total H_2O and CO_2 budgets in evolving magmas from
653 melt inclusion data. *Journal of Geophysical Research: Solid Earth*, *110*(B3).

654 Robie, R. A., & Hemingway, B. S. (1995). *Thermodynamic properties of minerals and related*
655 *substances at 298.15 K and 1 bar (10^5 Pascals) pressure and at higher temperatures* (No.
656 2131). US Government Printing Office.

657 Rust, A. C., & Cashman, K. V. (2004). Permeability of vesicular silicic magma: inertial and
658 hysteresis effects. *Earth and Planetary Science Letters*, *228*(1-2), 93-107.

659 Scaillet, B., & Macdonald, R. (2006). Experimental and thermodynamic constraints on the
660 sulphur yield of peralkaline and metaluminous silicic flood eruptions. *Journal of Petrology*,
661 *47*(7), 1413-1437.

662 Scaillet, B., & Macdonald, R. (2006). Experimental constraints on pre-eruption conditions of
663 pantelleritic magmas: evidence from the Eburru complex, Kenya Rift. *Lithos*, *91*(1), 95-108.

664 Scaillet, B., & Macdonald, R. A. Y. (2001). Phase relations of peralkaline silicic magmas and
665 petrogenetic implications. *Journal of Petrology*, *42*(4), 825-845.

666 Scaillet, B., & Macdonald, R. A. Y. (2003). Experimental constraints on the relationships
667 between peralkaline rhyolites of the Kenya Rift Valley. *Journal of Petrology*, *44*(10), 1867-
668 1894.

669 Scaillet, B., Holtz, F., & Pichavant, M. (1998). Phase equilibrium constraints on the viscosity
670 of silicic magmas: 1. Volcanic-plutonic comparison. *Journal of Geophysical Research: Solid*
671 *Earth (1978–2012)*, *103*(B11), 27257-27266.

672 Scaillet, B., Luhr, J. F., & Carroll, M. R. (2003). Petrological and volcanological constraints on
673 volcanic sulfur emissions to the atmosphere. *Volcanism and the Earth's atmosphere*, 11-40.

674 Sigl et al., 2022, Volcanic stratospheric sulfur injections and aerosol optical depth during the
675 Holocene (past 11 500 years) from a bipolar ice-core array, Earth Syst. Sci. Data, 14, 3167–
676 3196, 10.5194/essd-14-3167-2022.

677 Sigl, M., Winstrup, M., McConnell, J. R., Welten, K. C., Plunkett, G., Ludlow, F., ... &
678 Woodruff, T. E. (2015). Timing and climate forcing of volcanic eruptions for the past 2,500
679 years. *Nature*, *523*(7562), 543-549.

680 Sun, C., Plunkett, G., Liu, J., Zhao, H., Sigl, M., McConnell, J.R., Pilcher, J.R., Vinther, B.,
681 Steffensen, J.P. and Hall, V., 2014. Ash from Changbaishan Millennium eruption recorded in
682 Greenland ice: implications for determining the eruption's timing and impact. *Geophysical*
683 *Research Letters*, *41*(2), pp.694-701.

684 Taylor, B. E., Eichelberger, J. C., & Westrich, H. R. (1983). Hydrogen isotopic evidence of
685 rhyolitic magma degassing during shallow intrusion and eruption. *Nature*, *306*(5943), 541-
686 545.

687 Toulmin III, P., & Barton Jr, P. B. (1964). A thermodynamic study of pyrite and pyrrhotite.
688 *Geochimica et Cosmochimica Acta*, *28*(5), 641-671.

689 Wadsworth, F. B., Llewellin, E. W., Vasseur, J., Gardner, J. E., & Tuffen, H. (2020). Explosive-
690 effusive volcanic eruption transitions caused by sintering. *Science advances*, *6*(39),
691 eaba7940.

692 Wallace, P. J. (2001). Volcanic SO_2 emissions and the abundance and distribution of exsolved
693 gas in magma bodies. *Journal of Volcanology and Geothermal Research*, *108*(1), 85-106.

694 Wallace, P. J. (2005). Volatiles in subduction zone magmas: concentrations and fluxes based
695 on melt inclusion and volcanic gas data. *Journal of Volcanology and Geothermal Research*,
696 *140*(1), 217-240.

697 Wallace, P. J., & Gerlach, T. M. (1994). Magmatic vapor source for sulfur dioxide released
698 during volcanic eruptions: evidence from Mount Pinatubo. *Science*, *265*(5171), 497-499.

699 Wallace, P. J., Anderson, A. T., & Davis, A. M. (1999). Gradients in H_2O, CO_2, and exsolved gas
700 in a large-volume silicic magma system: Interpreting the record preserved in melt inclusions

from the Bishop Tuff. *Journal of Geophysical Research: Solid Earth (1978–2012)*, *104*(B9), 20097-20122.

Watkins, J. M., Manga, M., & DePaolo, D. J. (2012). Bubble geobarometry: A record of pressure changes, degassing, and regassing at Mono Craters, California. *Geology*, *40*(8), 699-702.

Wei, H., Liu, G., & Gill, J. (2013). Review of eruptive activity at Tianchi volcano, Changbaishan, northeast China: implications for possible future eruptions. *Bulletin of volcanology*, *75*(4), 1-14.

Wei, H., Wang, Y., Jin, J., Gao, L., Yun, S. H., & Jin, B. (2007). Timescale and evolution of the intracontinental Tianchi volcanic shield and ignimbrite-forming eruption, Changbaishan, Northeast China. *Lithos*, *96*(1), 315-324.

Westrich, H. R., & Gerlach, T. M. (1992). Magmatic gas source for the stratospheric SO_2 cloud from the June 15, 1991, eruption of Mount Pinatubo. *Geology*, *20*(10), 867-870.

White, J. C., Parker, D. F., & Ren, M. (2009). The origin of trachyte and pantellerite from Pantelleria, Italy: insights from major element, trace element, and thermodynamic modelling. *Journal of Volcanology and Geothermal Research*, *179*(1), 33-55.

Whitney, J. A. (1984). Fugacities of sulfurous gases in pyrrhotite-bearing silicic magmas. *American Mineralogist*, *69*(1-2), 68-78.

Xu, J., Liu, G., Wu, J., Ming, Y., Wang, Q., Cui, D., Shangguan, Z., Pan, B., Lin X., & Liu, J. (2012). Recent unrest of Changbaishan volcano, northeast China: a precursor of a future eruption?. *Geophysical Research Letters*, *39*, L16305, doi:10.1029/2012GL052600.

Xu, J., Pan, B., Liu, T., Hajdas, I., Zhao, B., Yu, H., ... & Zhao, P. (2013). Climatic impact of the Millennium eruption of Changbaishan volcano in China: New insights from high-precision radiocarbon wiggle-match dating. *Geophysical Research Letters*, *40*(1), 54-59.

Yang, Q., Jenkins, S.F., Lerner, G.A., Oppenheimer, C., Donovan, A., Hammond, J.O., Wei, H., Xu, J., Pan, B. and Nakanishi, R., 2022. A critical review of the sedimentary record of the Millennium Eruption'of Changbaishan/Paektu-san volcano.

Zhang, M., Guo, Z., Liu, J., Liu, G., Zhang, L., Lei, M., Zhao, W., Ma, L., Sepe, V. and Ventura, G., 2018. The intraplate Changbaishan volcanic field (China/North Korea): A review on eruptive history, magma genesis, geodynamic significance, recent dynamics and potential hazards. *Earth-Science Reviews*, *187*, 19-52.

Zhang, Y. (1999). H_2O in rhyolitic glasses and melts: measurement, speciation, solubility, and diffusion. *Reviews of Geophysics*, *37*(4), 493-516.

734 Zhao, B., Xu, J., Yu, H. and Chen, Z., 2020. Pyroclastic Density Current Facies in the
735 Millennium Eruption of Tianchi Volcano, Northeast China: Insights From Topography,
736 Stratigraphy, Granulometry, and Petrography. *Frontiers in Earth Science*, *8*, p.323.

737 Zou, H., Fan, Q., & Yao, Y. (2008). U–Th systematics of dispersed young volcanoes in NE
738 China: asthenosphere upwelling caused by piling up and upward thickening of stagnant
739 Pacific slab. *Chemical Geology*, *255*(1), 134-142.

740 Zou, H., Fan, Q., & Zhang, H. (2010). Rapid development of the great Millennium eruption of
741 Changbaishan (Tianchi) Volcano, China/North Korea: evidence from U–Th zircon dating.
742 *Lithos*, *119*(3), 289-296.

743 Zou, H., Fan, Q., Zhang, H., & Schmitt, A. K. (2014). U-series zircon age constraints on the
744 plumbing system and magma residence times of the Changbai volcano, China/North Korea
745 border. *Lithos*, *200*, 169-180.

746